

Measurement of Permittivity of Solid and Liquid Dielectrics in Coaxial Chambers

Antonije Đorđević, Jelena Dinkić, Marija Stevanović, Dragan Olćan,
Suzana Filipović¹, Nina Obradović¹

Abstract – We present two coaxial chambers for measurements of the complex permittivity of solid and liquid samples, in a frequency range that is in the transition between lower frequencies, where parallel-plate capacitor techniques are used, and higher (microwave) frequencies, where antennas, open coaxial lines, and waveguides are employed. Using a network analyzer, we measure the reflection coefficient of the chamber. From the obtained results, we extract the relative permittivity of the measured sample using a quasistatic or a dynamic model of the chamber with the sample.

Keywords – Measurements, Dielectrics, Electromagnetic fields, Numerical modeling, Coaxial line.

I. INTRODUCTION

Knowing electrical parameters of dielectrics is important not only for research and development in electrical engineering, but also in other areas, such as physical chemistry, medicine, and hydrology. Our motivation to deal with the characterization of dielectric materials came from our research in three distinct areas: sintered ceramic materials, three-dimensional (3-D) printed antennas, and microwave imaging of the human body.

The focus of this paper is on the characterization of solid and liquid dielectrics in the frequency domain, i.e., on the measurements of their complex relative permittivity. We assume the dielectric to be a linear, nonmagnetic material. The relative complex permittivity is usually expressed as $\epsilon_r = \epsilon'_r - j\epsilon''_r$, where ϵ'_r is the real part, j is the imaginary unit, and the imaginary part of the complex relative permittivity is $-\epsilon''_r$ (ϵ''_r is nonnegative for materials considered in this paper). The imaginary part comes from losses and it takes into account all dielectric losses: those due to the time-varying polarization and those due to the finite conductivity. (Instead by $-\epsilon''_r$, the dielectric losses are often characterized by the dielectric loss tangent, $\tan \delta = \epsilon''_r / \epsilon'_r$.) The real and the imaginary parts of the complex permittivity are functions of frequency. Due to the causality conditions [1], these functions must satisfy the Hilbert transform (or, equivalently, the Kramers-Kronig relations).

For the measurement of the dielectric parameters, there Antonije Đorđević, Jelena Dinkić, Marija Stevanović, and Dragan Olćan are with the University of Belgrade, School of Electrical Engineering, Bulevar kralja Aleksandra 73, 11020 Belgrade, Serbia, E-mails: edjordja@efz.bg.ac.rs, jdinkic@efz.bg.ac.rs, mnikolic@efz.bg.ac.rs, olcan@efz.bg.ac.rs

Suzana Filipović and Nina Obradović are with the Institute of Technical Sciences of SASA, Knez Mihailova 35/IV, 11000 Belgrade, Serbia, E-mails: suzana.filipovic@itn.sanu.ac.rs, nina.obradovic@itn.sanu.ac.rs

exist standard techniques and equipment [2]. The techniques depend on the frequency range, aggregate state of samples, as well as on the shape and size of available samples.

For measurements at lower frequencies, up to several hundred megahertz, the most commonly used technique is based on the measurement of the capacitance of a parallel-plate capacitor, where the sample is inserted between the capacitor electrodes. This technique is simple and convenient for measurements of solid samples in many cases. However, for high-permittivity samples (such as barium titanate and magnesium titanate), the accuracy of the method is reduced due to the formation of air gaps between the sample and the electrodes. Another problem is that for such samples the measurement structure cannot be assumed to be quasistatic already at about 100 MHz. At higher frequencies, internal resonances may occur in the sample and jeopardize the measurement accuracy.

At higher frequencies, the parallel-plate capacitor technique has another drawback due to the strong electromagnetic coupling with the environment. This coupling requires shielding. The shield, in turn, creates parasitic resonances. In order to suppress these resonances towards higher frequencies, it is convenient to keep the size of the shielded space as small as possible.

Finally, for a given dielectric that should be characterized, samples whose shape and dimensions are optimal for measurements are often not available. Examples are pill-shaped sintered samples [3], which practically cannot be machined or otherwise adapted to the measurement system. For example, commercially available meters (such as Agilent E4991A meter with Agilent 16451B probe) require that the sample has a large diameter (15 mm or more), whereas our samples of ceramic materials are much smaller (up to about 8 mm in diameter).

The parallel-plate capacitor measurement technique is convenient for the characterization of liquid dielectrics. The main limitation is the relatively low upper frequency limit.

For microwave frequencies (above about 1 GHz), open coaxial lines are often used to characterize various dielectrics [4]. Such a line is convenient because it usually does not require special forming of the sample. However, for accurate measurements, the sample should be big enough and it should be tightly positioned on the coaxial-line opening.

Microwave techniques based on the measurements of the transfer between two antennas [5] require relatively large samples. Similar techniques exist for measurements in coaxial and waveguide systems. However, they usually require that the samples have an appropriate shape and dimensions. For example, the Nicolson-Ross method [6] requires the sample to

completely fill out the cross section of the measurement coaxial line or waveguide.

For measurements of dielectric substrates in a wide frequency band, other techniques can be used [7], which also require a special shape of the dielectric or specific metallization shape on it.

Last but not least, in our circumstances, adequate equipment is often missing, particularly due to its very high cost. Hence, various radio-frequency and microwave measurements must be performed using available equipment and nonstandard, homemade sample holders.

All these problems have motivated us to develop a coaxial system (a coaxial chamber) for characterization of solid, pill-shaped samples, as well as a modification of this chamber that is designed for the measurements of parameters of liquid dielectrics. Electromagnetically, both systems are shielded from the environment. The measurement of the dielectric parameters is based on the measurement of the reflection coefficient of the chamber using a network analyzer, followed by the application of numerical techniques to extract the complex relative permittivity of the sample. The coaxial chambers presented in this paper are convenient for the characterization of dielectrics in the frequency range from about 10 MHz to 10 GHz.

This paper is an extension of our previous paper with the same title [8]. The present paper contains novel information about the numerical method for the electrostatic analysis, used to extract the dielectric parameters, a more detailed description of the model used for the SMA connector of the test fixture, and a description of a simple, open test fixture for characterization of solid dielectrics.

II. COAXIAL CHAMBERS

A. Chamber for Characterization of Solid Samples

Fig. 1 shows the coaxial chamber for characterization of solid samples. The chamber is made of brass and it has a rotational symmetry. A sample has the shape of a cylindrical pill, of diameter d and height h . In order to reduce the influence of air gaps when characterizing high-permittivity dielectrics, the upper and lower (flat) surfaces of the pill are painted by liquid silver and then dried in an oven for 1–2 h at 120 °C. Hence, the pill becomes a parallel-plate capacitor. When painting the pill, one should take care to prevent silver leakage over the lateral side of the cylinder, in order to maintain a well-defined shape of the electrodes.

The chamber is fed through an SMA connector with extended dielectric (Fig. 1b). The tip of the connector penetrates into the chamber and touches one electrode of the capacitor (pill). The other electrode rests on the chamber bottom. The bottom is a brass cylinder with a thread (i.e., a large screw). The cylinder can be taken out to insert the pill into the chamber. Three dielectric screws are provided to accurately position the pill in the chamber. These screws are removed from the chamber before measuring the reflection coefficient.

The reflection coefficient of the chamber is measured using a network analyzer: Agilent E5061A for the frequency range

between 300 kHz and 3 GHz, and Agilent N5227A for the frequency range between 1 GHz and 10 GHz. The reference (calibration) plane is shown in Fig. 1b.

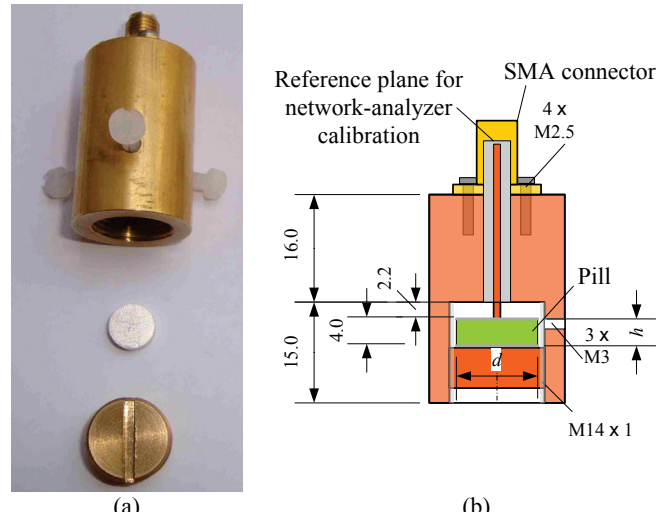


Fig. 1. Coaxial chamber for characterization of solid samples: (a) photo and (b) axial cross-section showing the position of the reference (calibration) plane for network-analyzer measurement. Dimensions are in millimeters

An accurate numerical model of the chamber and the sample is required in order to extract the dielectric parameters from the measured reflection coefficient. Several approaches were developed and tested. For lower frequencies, up to several hundred megahertz (depending on the relative permittivity and size: for higher permittivities and larger pills, the limit is lower), the model is quasistatic. It was developed by a modification of the electrostatic method presented in [9].

The original method from [9] was built for the numerical analysis of linear 3-D electrostatic systems that consist of arbitrary conducting and piecewise-homogeneous dielectric objects. In the analysis, the dielectric is replaced by the corresponding surface bound charges, located in a vacuum. Starting from the boundary conditions, a set of integral equations is formulated for the total charges (free plus bound) on surfaces of conducting bodies and on dielectric-to-dielectric interfaces. For the conducting bodies, the boundary condition is for the electrostatic potential. For the dielectric-to-dielectric interfaces, the boundary condition is for the normal component of the electrostatic-induction vector (electric flux density, \mathbf{D}), similar to the approach in [10]. The set of integral equations is solved using the method of moments [11]. More precisely, all boundary surfaces (of conductor and dielectrics) are patched in a set of polygonal patches. The total-charge distribution over each patch is approximated by an unknown constant. Dirac functions (impulses) are used for weighting, resulting in the point-matching method. Once the resulting system of linear equations is solved, the densities of the total charges are known for each patch.

For the evaluation of capacitances, the free charges (on the conductors) are required, and they have to be separated from the total charges. Let us consider an infinitesimally thin (zero-thickness) conductor, surrounded by two dielectrics (Fig. 2a).

The permittivity on one side of the conductor is ϵ_1 , and the permittivity on the other side is ϵ_2 . Starting from the boundary condition for the normal component of the electric field, the following equation for the surface density of the free charges (ρ_s) was derived in [10]:

$$\rho_s = \frac{\epsilon_2}{\epsilon_0} \rho_{st} + \mathbf{E}_1 \cdot \mathbf{n} (\epsilon_1 - \epsilon_2), \quad (1)$$

where ϵ_0 is the permittivity of a vacuum, ρ_{st} is the density of the total charges, \mathbf{E}_1 is the electric field on the conductor surface in the first dielectric, and \mathbf{n} is the unit normal from the second dielectric towards the first dielectric. This approach is implemented in both the 3-D software presented in [9] and the 2-D software in [10] because it provides a uniform treatment for both zero-thickness conductors and finite-thickness conductors.

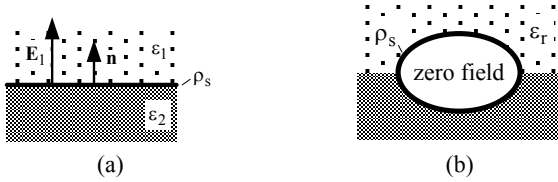


Fig. 2. (a) Zero-thickness conductor at interface between two dielectrics. (b) Finite-thickness conductor in piecewise-homogeneous dielectric

Eq. 1 gives excellent results in [10], where the Galerkin testing procedure is used in the method of moments. However, if the point-matching method is used, certain asymmetries are observed in the results, which violate the reciprocity. More precisely, if a multiconductor structure is analyzed, the matrix of the electrostatic-induction coefficients is not exactly symmetrical, in particular when a high-contrast between the dielectric permittivities is encountered. An even more pronounced problem was observed for the software from [9], when applied to electrostatic systems involving, for example, titanates (with the relative permittivity of the order of 100) and air. Hence, we had to modify the software from [9] to achieve the required symmetry, which would be within the computational accuracy of 1%.

The first modification was to use another condition instead of Eq. 1. We postulate here that all conductors have a finite thickness. If we consider a part of the conductor surface that is embedded in a dielectric of relative permittivity ϵ_r (Fig. 2b), we have simply

$$\rho_s = \epsilon_r \rho_{st}. \quad (2)$$

The drawback of this approach is that we must always have finite-thickness conductors in the numerical model, which in most cases increases the total number of unknowns. However, the symmetry of the results is now practically fully restored.

The second improvement is in using the Galerkin procedure instead of the point-matching method. The outer (Galerkin) integration is done numerically. This slows down the analysis, but significantly increases the accuracy of the results for a given meshing.

In order to extract the dielectric permittivity from the measured results, we need to optimize the permittivity of the

dielectric sample in the numerical model with the goal to match the numerical results for the capacitance with the measured results. This optimization can be very time-consuming. In order to expedite it, we have tabulated the capacitances for a set of diameters and heights of the pill:

- diameter (d) from 4 mm to 10 mm (step 0.5 mm);
- height (h) from 1 mm to 5 mm (step 0.4 mm);
- relative permittivity (ϵ_r) from 2 to 202 (step 50).

Thus, a large database was obtained. For a given diameter and height of the pill and for a given relative permittivity, we perform a three-dimensional linear interpolation within the database to find the corresponding capacitance, which is practically done in real time.

For higher frequencies, a detailed 3-D dynamic model was created using program WIPL-D [12].

In both programs, two models were created. The first model encompasses only the chamber. This model requires that the measured reflection coefficient (evaluated at the calibration plane) is transformed along the coaxial line formed by a part of the SMA connector and the chamber wall. The second model is more complex as it includes both the chamber and the complete SMA connector, all the way up to the calibration plane.

In both models, the SMA connector presented a serious problem. The connector was meticulously modeled by comparing results obtained by analytical models of a lossy coaxial line, results of measurements of coaxial SMA calibration standards, results of measurements of an open (empty) chamber (when the coaxial line is terminated only in the short tip of the SMA connector), and results of measurements of a short circuit placed at the entrance to the coaxial chamber (where the dielectric of the SMA connector terminates and the inner conductor enters the chamber). An accurate model of this coaxial line was essential for a reliable extraction of the dielectric parameters, in particular for evaluation of dielectric losses for low-loss samples.

The estimated relative permittivity of the dielectric of the SMA connector was estimated to be 1.95. It was established that the characteristic impedance of the coaxial line is only about 44Ω , instead of the expected 50Ω . The losses in the line are primarily due to the conductor losses. In order to accurately model these losses, it was necessary to perform a detailed analysis of the conductors. The basic material for the SMA connector is stainless (nonmagnetic) steel. It is plated by a thin layer of nickel, and then plated by gold. The thicknesses of gold and nickel are very small, so that the skin effect in gold and nickel is not pronounced at lower frequencies. Only at the highest frequencies involved here, the skin effect in gold takes over. Hence, for the analysis of the skin effect, an analytical model of a three-layer medium was made. Losses in steel dominate at lower frequencies. At frequencies about 1 GHz, losses in nickel dominate. Above 2 GHz, the losses in gold are prominent. In the model of the three-layer medium, the magnetic properties of nickel were taken into account, including the relaxation of the magnetization.

Fig. 3 shows the magnitudes of the reflection coefficient when the chamber is empty (open-circuited) and when the chamber is short-circuited, obtained by measurements and by modeling. The magnitude of the reflection coefficient of the

empty chamber (in dB), multiplied by -1 , approximately equals twice the attenuation along the coaxial line. When the chamber is short-circuited, in addition to the losses in the coaxial line, there are losses in the short circuit, but they were found to be relatively small. At frequencies up to around 2.5 GHz, the attenuation is much higher when coaxial line is short-circuited than when it is left open because the line is electrically short, so that there are much stronger currents in the first case, and, hence, the losses are larger [13].

For comparison, results obtained from three models are shown. In the first model, the SMA connector is assumed to be made only of stainless steel, of conductivity 10 MS/m. In this case, the conductor losses are significantly underestimated compared to the measured data.

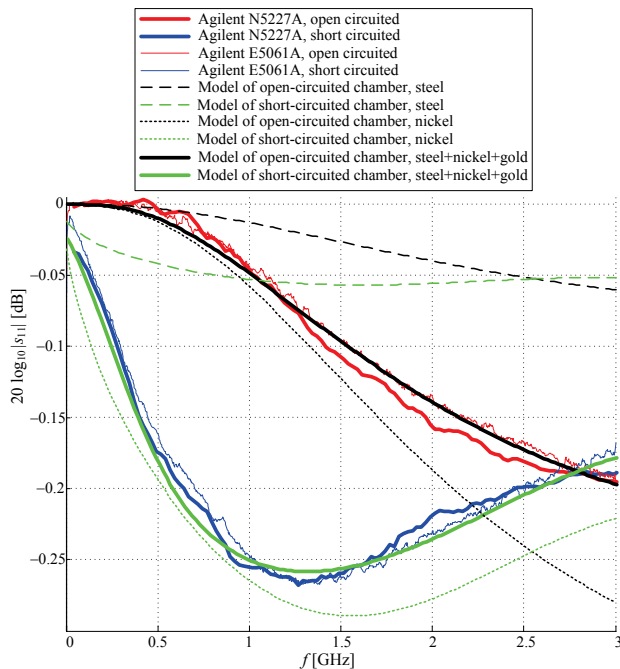


Fig. 3. Magnitudes of the reflection coefficient of empty chamber (open-circuited) and short-circuited chamber, obtained by measurements and modeling

In the second model, the SMA connector is assumed to be made only of nickel, of conductivity 14 MS/m and relative permeability 35. The permeability is assumed to diminish with frequency as a single-pole relaxation function with the cutoff at 2 GHz. The losses are significantly increased compared to the first model. For the open-circuited chamber, at lower frequencies, the computed attenuation follows relatively well the measured data. However, for the short-circuited chamber, the losses at frequencies below around 0.5 GHz are significantly overestimated. This can be explained by the fact that the skin depth at lower frequencies is, in reality, larger than the thickness of the nickel plating. The currents enter the steel core, which is nonmagnetic and its surface impedance is lower than that of nickel. The low-frequency behavior is improved if we take in the model that the core is made of steel with a thin layer of nickel (1 μm). However, Fig. 3 does not show the corresponding results. At frequencies above 1 GHz, this model also overestimates the losses. In reality, the low-

loss golden layer (estimated to be about 0.15 μm thick) takes over the bulk current, thus reducing losses.

In the third model, we use three layers: steel, nickel, and gold. For this model, we get the best agreement with the measured data not only up to 3 GHz (Fig. 3), but also beyond this frequency (Fig. 4).

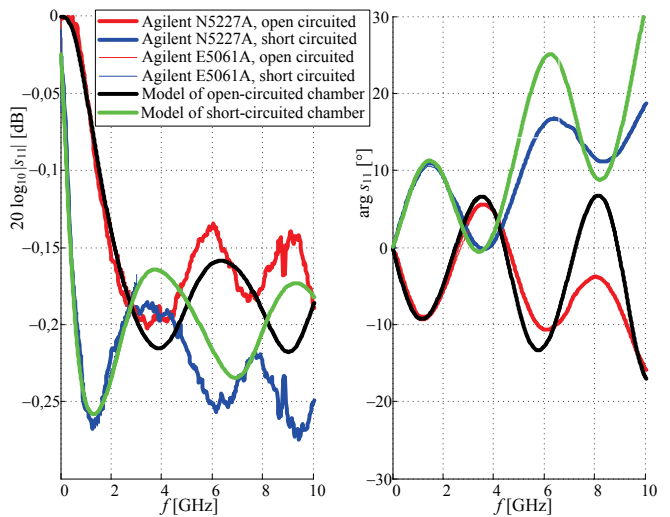


Fig. 4. Magnitudes and arguments of the reflection coefficient of empty chamber (open-circuited) and short-circuited chamber, in a wide frequency range, obtained by measurements and modeling

The model of the SMA connector is used to deembed the measured data, i.e., to transform the reflection coefficient measured at the calibration plane (Fig. 1) all the way down to the chamber entrance. (Although we have made numerical models for the chamber and the SMA connector as a unique electromagnetic structure, we present here results for models that involve only the chamber.)

The quasistatic model was used for measurements up to about 1 GHz. From the measured complex impedance, the complex impedance corresponding to the estimated parasitic inductance of the fixture is subtracted.

Using this model, we have established that the equivalent (complex) capacitance of chamber with the sample can be almost perfectly fitted by a linear function of the dielectric complex permittivity in a wide range of permittivities. This fact was verified both for low-permittivity samples (e.g., cordierite [14], [15]) and high-permittivity samples (e.g., magnesium titanate [16]). Hence, the extraction of the dielectric parameters is simple for lower frequencies. We take the geometrical data for the sample, evaluate its equivalent capacitance for two (assumed) relative permittivities using the database (the best policy is to take these two values so that the expected relative permittivity is in-between), and, finally, calculate the complex relative permittivity of the sample using a linear interpolation. Thus, although the data in the database are real values (computed for lossless cases), this procedure enables finding complex permittivities, provided the loss tangent is not overly large.

The extraction of parameters at higher frequencies is more complicated. We perform the dynamic analysis of the chamber and the sample for a two-dimensional array of points obtained by varying ϵ'_r and ϵ''_r (e.g., using a uniform step).

For each frequency for which the measurements are performed, we evaluate the parameters ϵ'_r and ϵ''_r by applying a two-dimensional interpolation within the grid of the computed data. We also employ an alternative procedure by varying ϵ'_r and ϵ''_r using an optimization method so to make the simulation results as close as possible to the measured values of the reflection coefficient. In any case, the results of the extraction are the parameters ϵ'_r and ϵ''_r as a function of frequency.

For comparison, we have also produced a simple, classical test fixture, sketched in Fig. 5. It consists of a standard SMA connector and an elastic metallic plate. The dielectric pill is inserted between the pin of the SMA connector and the plate. In the measurement procedure, the network analyzer is calibrated at the standard cross section of the SMA connector. Thereafter, the pin is short-circuited to the body of the connector, and the calibration plane is moved to the other end of the SMA connector, where the short circuit is located (i.e., we apply the port extension). The sample is inserted into this fixture and the impedance is measured. The estimated influences of the parasitic inductance and the parasitic capacitance of the pin are subtracted. The pill is modeled in a similar way as the coaxial chamber with the pill, using the quasistatic approach. Using this model, the relative complex permittivity of the sample is estimated.

This fixture was also used to measure the sample using an impedance meter. Thereby, the capacitance of the empty test fixture was measured. The pill was inserted, the capacitance was measured, and the capacitance of the empty fixture was subtracted. The conductance was also measured, but no correction was made for dielectric losses in the test fixture, as these losses were found to be negligible.

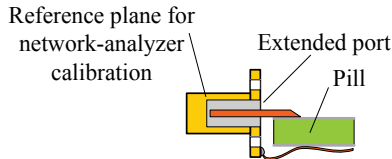


Fig. 5. Classical test fixture

Fig. 6 shows the parameters ϵ'_r and $\tan\delta$ for cordierite (which is a low-permittivity material), and Fig. 7 shows the parameters ϵ'_r and ϵ''_r for magnesium titanate (which is a high-permittivity material). Note that the relative permittivity of magnesium titanate has a very large imaginary part. Figs. 6 and 7 show computed results obtained by the quasistatic model. Fig. 7 also shows results computed using the dynamic model. In addition, Figs. 6 and 7 show results obtained using the classical test fixture shown in Fig. 5. Fig. 7 also shows results for frequencies below 10 MHz obtained by the impedance meter Hewlett Packard HP4192A. The present technique breaks down at lower frequencies because the impedance is very large in magnitude and thus very difficult to be measured by network analyzers (Fig. 6). At frequencies above around 1 GHz, the quasistatic model breaks down both for the proposed coaxial chamber and the classical test fixture (Fig. 7) and parasitic resonances occur. The dynamic model is

flawless at higher frequencies (Fig. 7), but the corresponding computation time is significant.

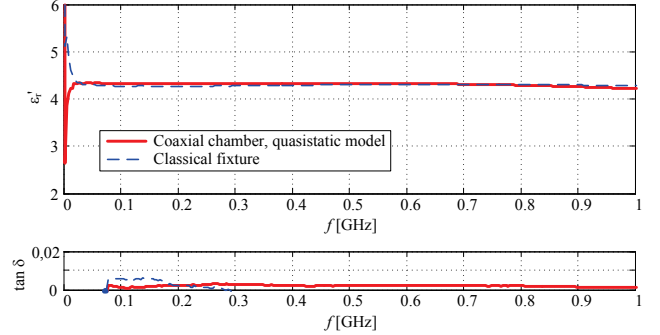


Fig. 6. Real part of the relative complex permittivity and the loss tangent for sintered cordierite, as a function of frequency.

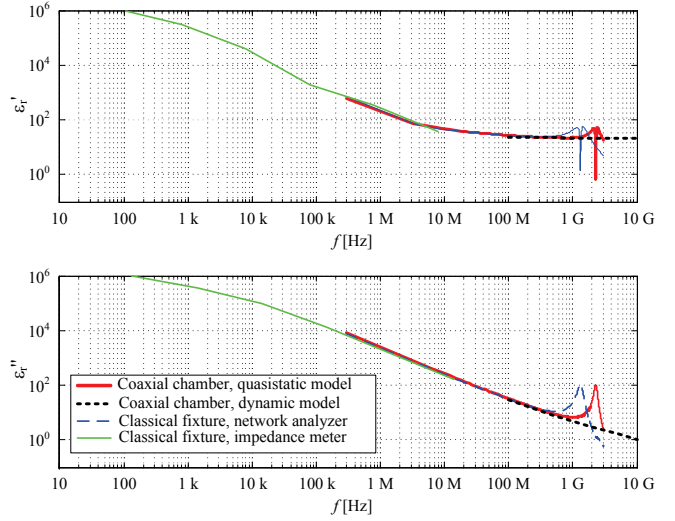


Fig. 7. Real part and negative of the imaginary part of the relative complex permittivity of sintered magnesium titanate, as a function of frequency

B. Chamber for Characterization of Liquid Samples

Fig. 8 shows a modification of the coaxial chamber suitable for measurements of the relative permittivity of liquid dielectrics. The construction of the chamber is similar to that shown in Fig. 1. However, the bottom of the chamber is open now, so that the chamber can be vertically immersed into a liquid sample located in a container. The chamber shown in Fig. 8 also has an SMA connector with extended dielectric. However, a large part of the dielectric is now removed. The bare part of the inner conductor of the SMA connector plays the role of the inner conductor of the coaxial chamber and it is in contact with the liquid sample. There are three small holes at the top of the chamber. Their purpose is to let air out, so that the chamber can be completely filled out with the liquid. The SMA connector is protected from flooding by the cylindrical rim of the chamber.

The chamber for the characterization of liquid dielectrics is modeled using the same techniques as the chamber for solid samples. The quasistatic model is used for lower frequencies, and the dynamic model for the higher frequencies. In the latter case, for modeling of high-permittivity dielectrics (such as

water and ethanol), it was found useful to use measured data transformed to the chamber entrance. In this case, we can take that the complete metallic structure is located in an infinite homogeneous medium, having identical parameters as the measured liquid. This can be done because the electromagnetic field outside the chamber is negligible (except at very high frequencies, when the chamber begins to radiate). Such an approach significantly contributes to the numerical stability of the electromagnetic model because high contrasts between pairs of adjacent dielectric domains are avoided.

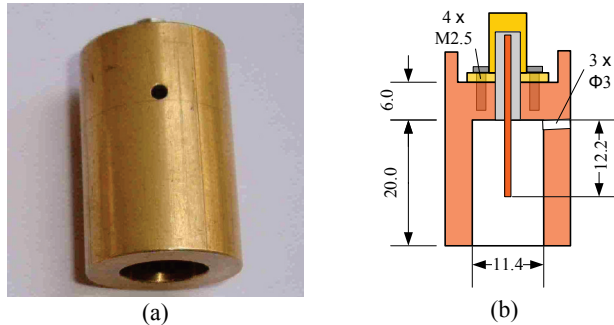


Fig. 8. Coaxial chamber for characterization of liquid samples: (a) photo and (b) axial cross-section. Dimensions are in millimeters

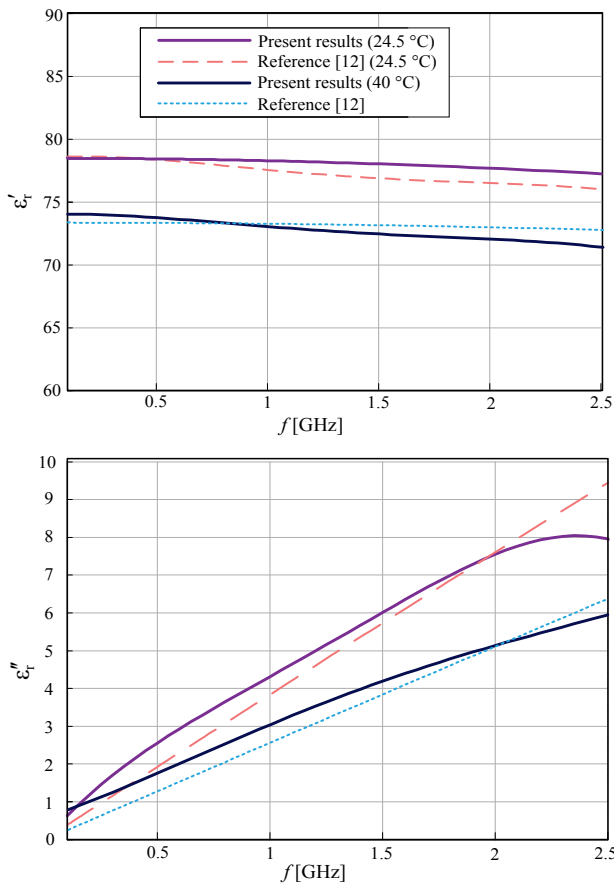


Fig. 9. Real part and negative of the imaginary part of the relative complex permittivity of distilled water at 24.5 °C and 40 °C, as a function of frequency

As an example of measurements of high-permittivity liquid dielectrics, Fig. 9 displays results for ϵ_r' and ϵ_r'' for distilled water at 24.5°C and 40°C obtained by the presented method, in comparison with the data from [17]. For both temperatures, a good agreement was obtained between the two sets of results.

III. CONCLUSIONS

The paper presents coaxial chambers for measurement of the complex relative permittivity of solid and liquid dielectric samples. The chambers are convenient for characterization of small samples, at frequencies where the classical parallel-plate method starts to break down. Within a single measurement sweep, it is possible to encompass a wide frequency range, from several MHz to several GHz. We have designed the chamber for solid samples in order to be able to characterize sintered ceramic materials, and the chamber for liquid samples for measurements of liquids that model biological tissues in phantoms used for microwave imaging.

ACKNOWLEDGEMENT

This work was supported in part by the Project TR32005 financed by the Ministry of Education, Science and Technological Development of the Republic of Serbia.

This is an extended version of the paper “Measurement of Permittivity of Solid and Liquid Dielectrics in Coaxial Chambers” presented at the 60th Conference on Electrical, Electronic and Computing Engineering ETRAN 2016, held in June 2016 on Zlatibor, Serbia. The paper has been awarded as the best paper presented in the Section Antennas and Propagation.

REFERENCES

- [1] A.R. Đorđević, D.V. Tošić, “Causality of Circuit and Electromagnetic-field Models”, *5th European Conference on Circuits and Systems for Communications (ECCSC'10)*, pp. 12-21, Belgrade, Serbia, 2010.
- [2] O.V. Tereshchenko, F.J.K. Buesink, F.B.J. Leferink, “An Overview of the Techniques for Measuring the Dielectric Properties of Materials”, *General Assembly and Scientific Symposium*, vol. 1320, pp. 1-4, Istanbul, Turkey, 2011.
- [3] N. Obradović, M.V. Nikolić, N. Nikolić, S. Filipović, M. Mitić, V. Pavlović, P.M. Nikolić, A.R. Đorđević, M.M. Ristić, “Synthesis of Barium-zinc-titanate Ceramics”, *Science of Sintering*, vol. 44, no. 1, pp. 65-71, 2012.
- [4] T.P. Marsland, S. Evans, “Dielectric Measurements with an Open-ended Coaxial Probe”, *IEE Proc. Microw., Antennas Propag.*, vol. 134, pp. 341-349, 1987.
- [5] D.K. Ghodgaonkar, V.V. Varadan, “A Free-space Method for Measurement of Dielectric Constants and Loss Tangents at Microwave Frequencies”, *IEEE Trans. Instrum. Meas.*, vol. 37, no. 3, pp. 789-793, 1989.
- [6] A.M. Nicolson, G.F. Ross, “Measurement of the Intrinsic Properties of Materials by Time Domain Techniques”, *IEEE Trans. Instrum. Meas.*, vol. IM-19, no. 4, pp. 377-382, 1970.
- [7] A.R. Djordjević, R.M. Biljić, V.D. Likar-Smiljanić, T.K. Sarkar, “Wideband Frequency-Domain Characterization of FR-

- 4 and Time-Domain Causality”, *IEEE Trans. Electromagn. Compat.*, vol. 43, no. 4, pp. 662-667, 2001.
- [8] A. Đorđević, J. Dinkić, M. Stevanović, D. Olćan, S. Filipović, N. Obradović, “Measurement of Permittivity of Solid and Liquid Dielectrics in Coaxial Chambers”, *60th Conference on Electrical, Electronic and Computing Engineering ETRAN 2016*, paper AP1.2, Zlatibor, Serbia, 2016.
- [9] D.I. Olćan, I.M. Stevanović, J.R. Mosig, A.R. Djordjević, “Diakoptic Surface Integral Equation Formulation Applied to 3-D Electrostatic Problems”, *ACES 2007*, pp. 492-498, Verona, Italy, 2007.
- [10] A.R. Djordjević, M.B. Baždar, R.F. Harrington, T.K. Sarkar, *LINPAR for Windows: Matrix Parameters for Multiconductor Transmission Lines*, Boston, MA, Artech House, 1999.
- [11] R.F. Harrington, *Field Computation by Moment Methods*, Hoboken, NJ, Wiley-IEEE Press, 1993.
- [12] WIPL-D Pro 3-D, <http://www.wipl-d.com/>
- [13] A.R. Djordjević, A.G. Zajić, D.V. Tošić, T. Hoang, “A Note on the Modeling of Transmission-line Losses”, *IEEE Trans. Microw. Theory Techn.*, vol. 51, no. 2, pp. 483-486, 2003.
- [14] N. Obradović, S. Filipović, N. Đorđević, D. Kosanović, S. Marković, M. Mitić, V. Pavlović, D. Olćan, A. Djordjević, M. Kachlik, K. Maca, “Effects of Mechanical Activation and Two-step Sintering on Structure and Electrical Properties of Cordierite-Based Ceramics”, *Ceramics International*, vol. 42, no. 12, pp. 13909-13918, 2016.
- [15] N.N. Obradović, *Synthesis of Cordierite-Based Ceramics*, Belgrade, Serbia, Academic Mind, 2016.
- [16] S. Filipović, N. Obradović, V. B. Pavlović, M. Mitić, A. Đorđević, M. Kachlik, K. Maca, “Effect of Consolidation Parameters on Structural, Microstructural and Electrical Properties of Magnesium Titanate Ceramics”, *Ceramics International*, vol. 42, no. 8, pp. 9887-9898, 2016.
- [17] W.J. Ellison, “Permittivity of Pure Water at Standard Atmospheric Pressure over the Frequency Range 0–25 THz and the Temperature Range 0–100 °C”, *J. Phys. Chem. Ref. Data*, vol. 36, no. 1, pp. 1-18, March, 2007.